

Cite this: DOI: 10.1039/c9dt04827h

S-Doped three-dimensional graphene (S-3DG): a metal-free electrocatalyst for the electrochemical synthesis of ammonia under ambient conditions†

Jin Wang,^a Shuang Wang ^{*a,b} and Jinping Li ^{*b}

In this study, we report sulfur-doped three-dimensional graphene (S-3DG) as a metal-free electrocatalyst for N₂ reduction reaction (NRR) under ambient conditions. Due to the high electron transport capacity and stable physicochemical properties of 3DG, it was utilized to improve the NRR catalytic performance dramatically. Hence, in 0.05 M H₂SO₄ the S-3DG achieved a remarkably large NH₃ yield of 38.81 μg_{NH₃} mg_{cat}⁻¹ h⁻¹ and a high faradaic efficiency of 7.72% at -0.6 V versus a reversible hydrogen electrode (RHE), which is superior to most non-metal catalysts. Notably, it shows such outstanding selectivity that no hydrazine by-products were detected and the electrochemical stability passed a long-term durability test.

Received 20th December 2019,
Accepted 17th January 2020

DOI: 10.1039/c9dt04827h

rsc.li/dalton

Introduction

Ammonia is a very important chemical raw material, which is mainly used in chemical fertilizer production, chemical industry, medicine, and other fields.^{1–3} The Haber–Bosch process, as the main method of the industrial production of ammonia, produces over 150 million metric tons of ammonia each year while consuming 1–2% of the global energy supply and emits over 450 million metric tons of CO₂ annually.^{4,5} Hence, it is urgent to find a sustainable way to replace the conventional process. Compared to the harsh production conditions of the traditional methods, electrocatalysis is promising as it is driven by electric energy and thus, it can make the reaction of the ammonia synthesis free from or less restricted by thermodynamic equilibrium.^{6,7}

Electrocatalysis is the core and key of technological progress, energy saving, and emission reducing in an electrochemical ammonia synthesis. At present, the research on electrocatalysts for N₂ fixation can be divided into the following three categories: precious metal, non-precious metal, and non-metal.^{8–10} The research on the electrocatalytic properties of precious metals as electrocatalysts was carried out earlier, such as Au, Ru, and Rh.^{11,12} Until now, there have been in-depth researches on precious metal catalysts and some achievements

have been made, for example Ziqiang Wang *et al.* reported flower-like Au as efficient electrocatalysts for the NRR and gained a high performance, in which the NH₃ yield rate was 25.57 μg_{NH₃} mg_{cat}⁻¹ h⁻¹ and the FE was 6.05% at -0.2 V in 0.1 M HCl.^{13–18} However, limited by costs and scarce resources, scientists have turned their attention to non-precious metals such as Mn, Co, and Gr; for instance, the CoS₂/NS-G hybrid shows a high yield rate and superior faradaic efficiency for NH₃ production.¹⁹ The highest faradaic efficiency of 25.9% was achieved at -0.05 V vs. RHE, while the highest yield of 25.0 μg_{NH₃} mg_{cat}⁻¹ h⁻¹ was obtained at -0.2 V vs. RHE.²⁰ However, the metal ions that are released by the metal catalyst are unmanageable apart from the high cost.^{21–23} X. Sun *et al.* proved that the multishelled hollow Cr₂O₃ microspheres achieved a high faradaic efficiency (6.78%) and a large NH₃ yield (25.3 μg_{NH₃} mg_{cat}⁻¹ h⁻¹) at -0.9 V but the degradation of Cr³⁺ takes more time and energy.²⁴ Therefore, scientists urgently need to find a sustainable material to replace it, such as non-metals. Subsequently, papers have been published progressively using P, B, and S as the catalytic center for NRR.^{19,25} X. Sun *et al.* published boron as the active center that gave an ideal result (13.22 μg_{NH₃} mg_{cat}⁻¹ h⁻¹, 4.04% and 14.4 μg_{NH₃} mg_{cat}⁻¹ h⁻¹, 3.4%) at -0.8 V in 0.1 M Na₂SO₄.^{26,27} Nevertheless, the performance of most non-metals catalysts is unsatisfactory because they are natural electrical insulators, which greatly obstructs the electron mass transfer and directly leads to the sharp drop in the nitrogen conversion yield and electron utilization rate.^{28–32} The best and most direct way to improve this situation is to use conductive substrates, such as carbon material.^{33–37}

Graphene, as a material that has high electron transport capacity, high specific surface area, and high physicochemical

^aCollege of Environmental Science and Engineering, Taiyuan University of Technology, Jinzhong 030600, Shanxi, P.R. China. E-mail: wangshuang@tyut.edu.cn

^bShanxi Key Laboratory of Gas Energy Efficient and Clean Utilization, Taiyuan University of Technology, Taiyuan 030024, Shanxi, P.R. China

†Electronic supplementary information (ESI) available. See DOI: 10.1039/c9dt04827h

stability, stands out amongst many carbon substrates and is usually selected to act as an optimal dopant apply to load the non-metal for NRR to improve the electron conduction ability of the non-metallic catalyst.^{19,20,31,32,38–40} In 2012, Shi Zhang Qiao *et al.* demonstrated that the synergistic enhancement of thio-nitrogen co-doped mesoporous graphene electrocatalysts in oxygen reduction results from the redistribution of spin and charge densities brought about by the dual doping of S and N atoms, which leads to a large number of carbon atom active sites over graphene.⁴¹ Zhixiong You *et al.* reported Ru nanocrystallites on graphene substrate, which enhanced the NRR by the formation of ruthenium–carbon bonds between graphene and ruthenium coordination compounds, thus showing that graphene has a promising future in ammonia synthetic catalysts.⁴² 3D-graphene does not only have excellent properties of graphene but also the unique three-dimensional network structure, which provides more channels for electron transport, more specific surface areas spread over the catalyst evenly, and makes the physicochemical properties more stable, thus improving the nitrogen reduction performance.⁴³

Herein, we have reported graphene with a unique three-dimensional structure^{43–47} as the substrate of the supported catalyst, which loaded sulfur (S-3DG) at low temperature that acts as an efficient NRR catalyst for electrochemical nitrogen fixation at ambient conditions and provided a satisfactory yield and FE, which were 38.81 $\mu\text{g}_{\text{NH}_3}$ $\text{mg}_{\text{cat}}^{-1} \text{h}^{-1}$ and 7.72%, respectively, in 0.05 M H_2SO_4 at -0.6 V. Moreover, the catalyst demonstrates such superior selectivity that hydrazine was not detected in the product and long-term durability for the reaction.

2. Experimental section

2.1 Materials

Sodium gluconate ($\text{C}_6\text{H}_{11}\text{NaO}_7$, 99.0%), sodium sulfate (Na_2SO_4 , 99.0%), hydrochloric acid (HCl, 99.0%), ammonium chloride (NH_4Cl), salicylic acid ($\text{C}_7\text{H}_6\text{O}_3$), sodium citrate dehydrate ($\text{C}_6\text{H}_5\text{Na}_3\text{O}_7 \cdot 2\text{H}_2\text{O}$), *p*-dimethylamino-benzaldehyde ($\text{C}_9\text{H}_{11}\text{NO}$), sodium nitroferricyanide dehydrate ($\text{C}_5\text{FeN}_6\text{Na}_2\text{O} \cdot 2\text{H}_2\text{O}$), and sodium hypochlorite solution (NaClO) were purchased from Aladdin Ltd (Shanghai, China). Nafion (5 wt%) solution was purchased from Sigma-Aldrich Chemical Reagent Co., Ltd. Hydrochloric acid, nitric acid, sulfuric acid, hydrogen peroxide, hydrazine monohydrate ($\text{N}_2\text{H}_4 \cdot \text{H}_2\text{O}$), and ethyl alcohol ($\text{C}_2\text{H}_5\text{OH}$) were purchased from Sinopharm Chemical Reagent Co., Ltd, China. The ultrapure water used throughout all experiments was purified through a Millipore system. The high-purity nitrogen and argon gases used in the experiment, as well as other experimental gases, all came from Anxuhongyun Technology Development Co. Ltd. All the reagents were analytical reagent grade and were used without further purification.

2.2 GO preparation

GO was prepared using the classic Hummers' method, which uses flake graphite powder as the carbon source. Simply, 46 mL concentrated sulfuric acid was poured into a 250 mL

round-bottom flask containing flake graphite powder and the mixture was magnetically stirred in an ice water bath. Then, the same was magnetically stirred in an oil bath at 35 °C for 2 h. After this, 92 mL of ultra-pure water was added, followed by stirring at 98 °C for 15 minutes. Then, 280 mL ultra-pure water and 5 mL hydrogen peroxide were added into the mixed solution successively after the solution was naturally cooled to room temperature. After that, the mixture was pumped and filtered by a circulating water pump; meanwhile, 500 mL 10% hydrochloric acid solution was slowly added. The product was transferred to a centrifuge tube, diluted with ultrapure water, and centrifuged at 10 000 rpm for 20 min until the supernatant was neutral. The diluted sediment was put into a dialysis bag and dialysis was carried out for 7 days. The ultrasonic dispersion of the suspended solution after dialysis was conducted at 120 W power by an ultrasonic cell grinder for 30 minutes, followed by centrifugation at 10 000 rpm; the upper liquid obtained was the graphene oxide-water suspension, which was diluted with water to a concentration of 5 mg mL^{-1} .

2.3 3D-graphene preparation

The concentration of 5 mg mL^{-1} of graphene oxide in 5 mL water suspension kept in 20 mL glass samples in the bottle was measured and 100 μL hydrazine hydrate and 17.5 μL ammonia were added; the samples of glass bottles were then put in a 100 mL PTFE autoclave tank with a sealed stainless steel shell and heated to 180 °C in the drum wind drying oven temperature reaction for 3 h to obtain quick black cylindrical 3D-graphene hydrogels.

2.4 S-3DG preparation

A 3D-graphene hydrogel was immersed in sodium thiosulfate solution ($\text{Na}_2\text{S}_2\text{O}_3$, 2.5 M, 50 mL) at the ambient temperature of 60 °C under magnetic stirring for 5 h. After the reaction, the container was placed in the refrigerator and pre-frozen. Half an hour later, the same pre-frozen mixture (HCl, 1 M, 6 mL) was added to the solution drop by drop under magnetic stirring at 500 rpm. The as-obtained sulfur–graphene hydrogels were washed several times and then subjected to oven drying at 150 °C for 12 h to produce sulfur–graphene gels.

2.5 Electrode preparation

2 mg of the catalyst was dispersed in 960 μL ($V_{\text{water}} : V_{\text{ethanol}} = 1 : 2$) mixed solution and 40 μL Nafion solution (5 wt%) was sonicated for at least 40 min to form a homogeneous ink. Then, 50 μL of the catalyst ink was drop-casted onto carbon paper with a loading of 0.1 mg. The area of carbon paper electrode was $1 \times 1.5 \text{ cm}^2$ and the practically immersed area in the electrolyte was $1 \times 1 \text{ cm}^2$. It was allowed to dry naturally and left under a baking lamp for 1 h, then dipped in the prepared electrolyte for 1 h. The working electrode was ready to be used.

2.6 Characterizations

SEM images were collected from a tungsten lamp-equipped SU8010 scanning electron microscope at an accelerating

voltage of 20 kV (HITACHI, Japan). The crystal structures of the synthesized samples were analyzed on a Rigaku Mini Flex II benchtop powder X-ray diffractometer (XRD) with Cu-K α radiation (40 kV, 40 mA, $\lambda = 0.15418$ nm) in the 2θ range of 5–80° with a scanning rate of 8° min⁻¹. The morphologies of the samples were observed by scanning electron microscopy (Hitachi, SU8010). Transmission electron microscopy (TEM) was carried out on a JEM-2100F instrument. The X-ray photoelectron spectroscopy (XPS) measurements were performed on a Thermo Fisher Scientific K-Alpha spectrometer with Al K α (1486.6 eV) as the X-ray excitation source. Thermogravimetric analysis was carried out with a heating rate of 5 K min⁻¹ from 303 K to 1273 K in N₂ on STA 449 F5 obtained from the NETZSCH company. The absorbance data of the spectrophotometer were measured on a PerkinElmer Lambda 650 ultraviolet-visible (UV-Vis) spectrophotometer.

2.7 Electrochemical measurements

The electrochemical tests were carried out in a three electrode system on an electrochemical workstation (VERSASTAT3) at room temperature. The electrochemical reduction of N₂ to ammonia was performed in a two-compartment cell at room temperature and the cells were separated by a Nafion 117 membrane. An Ag/AgCl (saturated KCl solution) electrode was used as the reference electrode and a platinum foil electrode was used as the counter electrode. The electrolyte volume in the two parts of the H-cell was 70 mL. For electrocatalytic N₂ reduction, potentiostatic tests were conducted in N₂-saturated 0.05 M H₂SO₄ for 2 h, which was purged with N₂ for 30 min before the measurement. Pure N₂ was continuously fed into the cathodic compartment with a properly positioned sparger during the experiments.

3. Results and discussion

3.1 Structural and morphological analysis

S-3DG was prepared by the following reaction: Na₂S₂O₃ + 2HCl → S↓ + 2NaCl + H₂O + SO₂↑. Note that sulfur was loaded on the surface of 3D-graphene in an ice bath to undergo interfacial growth. Then, a certain number of carbon–sulfur bonds were formed between them at a high temperature maintained at for 10 hours. The scanning electron microscopy (SEM) images show that the S-3DG samples (Fig. 1b) maintain the intrinsic interlinked porous network of 3D-graphene (Fig. 1a) well with even more fold morphologies, which are indicative of unique characteristics including large folded morphology, which results in higher specific surface areas and morphology stability. The distribution of C and S elements is shown in Fig. 1f and g, respectively. The distribution mapping shows that sulfur was evenly distributed across the graphene sheets; thus, the uniformity of doping is proved. The TEM images of 3D-graphene (Fig. 1c) and S-3DG (Fig. 1d) were measured with the same magnification. Obviously, in S-3DG, there were large black shaded areas because of sulfur doping in contrast with Fig. 1c. The significant doping of sulfur in the 3D graphene was successfully and uniformly demonstrated.

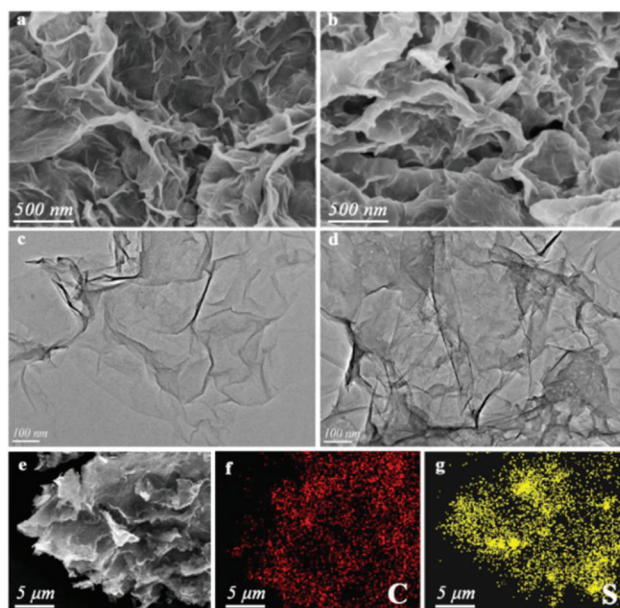


Fig. 1 SEM of (a) 3D-graphene and (b) S-3DG and TEM of (c) 3D-graphene and (d) S-3DG (e–g) SEM and EDS elemental mapping images of C and S for S-3DG.

3.2 Raman analysis

By comparing the Raman spectra of 3D-graphene (Fig. S5†) and S-3DG (Fig. 2), we can calculate that the I_D/I_G of S-3DG is higher than that for 3D-graphene, which demonstrates that S-3DG has more defects due to sulfur doping where the D characteristic peak represents the defects in graphene and the G characteristic peak indicate that sp² carbon atoms vibrate in the plane. The increase in the defect sites is more conducive for nitrogen adsorption and dissociation.

3.3 XRD analysis

The X-ray diffraction (XRD) patterns of 3D-graphene and S-3DG are displayed in Fig. 3, the diffraction peaks at 23.7° corresponding to the (002) plane of 3D-graphene and the bulge confirmed the amorphous nature of 3D-graphene.

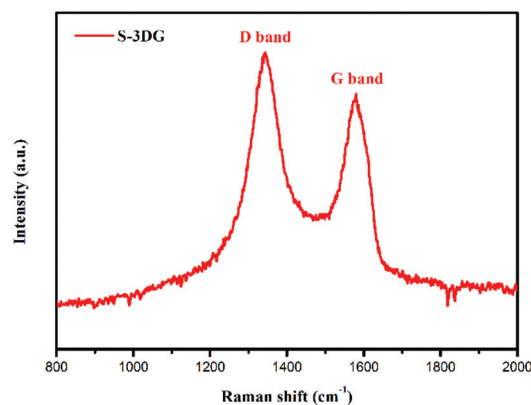


Fig. 2 Raman spectrum of S-3DG.

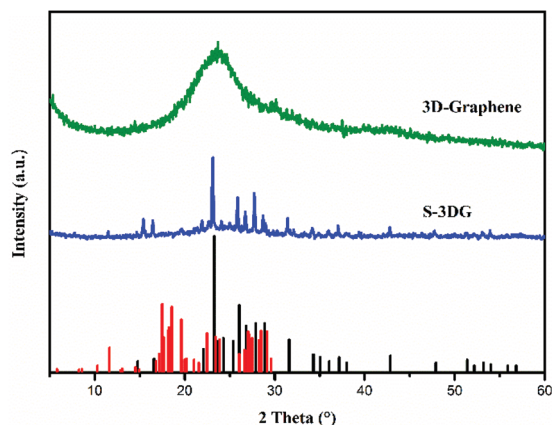


Fig. 3 XRD patterns of 3D-graphene and S-3DG.

Compared with 3D-graphene, the diffraction peaks of S-3DG clearly corresponded to the PDF card (PDF 52-0976 red and PDF 42-1278 black), which is consistent with the carbon-sulfur compound and pristine S, respectively. Hence, the result of XRD also qualitatively demonstrates the successful doping of sulfur in 3D-graphene. The quantitative measurement of sulfur doped was done by thermogravimetry (TG) and the results in Fig. S6† show that the sulfur content of S-3DG is up to 68.8%, in which most of it is in the form of elemental sulfur and few of it is in the form of carbon-sulfide compound, which combines the result of EDS (Fig. S7†) after the TG testing is completed (Table S1†).

3.4 XPS analysis

X-ray photoelectron spectra (XPS) for S-3DG for C 1s and S 2p is shown in Fig. 4a and b, respectively. In the C 1s region (Fig. 4a), the peaks at the binding energies (BEs) of 284.7, 285.3, and 289.2 eV are assigned to C-C/C=C, C-S/C-O, and O=C-O carboxyl groups, respectively. The S 2p spectrum (Fig. 4b) can be resolved into three peaks at BEs of 164.0, 165.2, and 168.8 eV, which are assigned to the -C-S-C-, -C-S-, and -C-SO_x (*x* = 2, 3, and 4) species, respectively. The XPS for 3DG, as a comparison data, is shown in Fig. S9† to prove that there was no sulfur in raw 3DG. Moreover, we did low concentration comparisons to get the suitable sulfur source concentration and the XPS spectra for S-3DG (1 M Na₂S₂O₃) for C 1s and S 2p is shown in Fig. S10,† the characteristic peaks of the C-S bond can be clearly seen from the map. The XPS data also fully demonstrates that sulfur was doped in 3D-Graphene in the form of elemental sulfur and carbon-sulfide compound successfully.

3.5 Electrocatalytic performance for ammonia synthesis

The experiment used a classical H-type electrolytic cell, which was separated by a Nafion membrane in 0.05 M H₂SO₄ and with three-electrode configuration at the ambient temperature. S-3DG was dispersed in a mixture of ultrapure water and ethanol in the ratio of 1:2 (vol%) and the ink was doped on carbon paper as the working electrode, Ag/AgCl and platinum

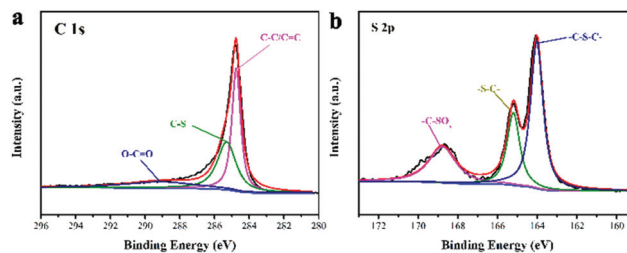


Fig. 4 XPS spectra for S-3DG in the (a) C 1s and (b) S 2p regions.

plate electrode as reference electrode and counter electrode, respectively. In this paper, unless otherwise specified, all the reported potentials were converted to values *versus* RHE. The electrocatalytic NRR activity of S-3DG was tested using controlled potential electrolysis in N₂-saturated electrolyte for 2 h. Fig. 5a shows the linear sweep voltammetric (LSV) curves for S-3DG/CP in Ar- and N₂-saturated 0.05 M H₂SO₄. It obviously shows that S-3DG/CP display a higher current density in N₂-saturated solution than in Ar-saturated solution, which indicated the high activity towards NRR. For electrocatalysts, stability is an important index; the result of the long-term durability measurement test of S-3DG/CP for 20 h is shown in Fig. 5b, which proved the expected stability of S-3DG/CP. Also, Fig. 5c displays the chronoamperometric curves of S-3DG/CP at different potentials from -0.8 to -0.4 V for 2 h. To compare, the same loading quantity of 3DG/CP was also tested for electrochemical reaction under the same conditions, as displayed in Fig. 5d. Meanwhile, a comparison diagram of the yield under argon and open circuit voltage is also shown in Fig. 5d. According to a report in the literature, in order to eliminate the experimental error due to the repeated use of the membrane for the deposition of ammonia released into the

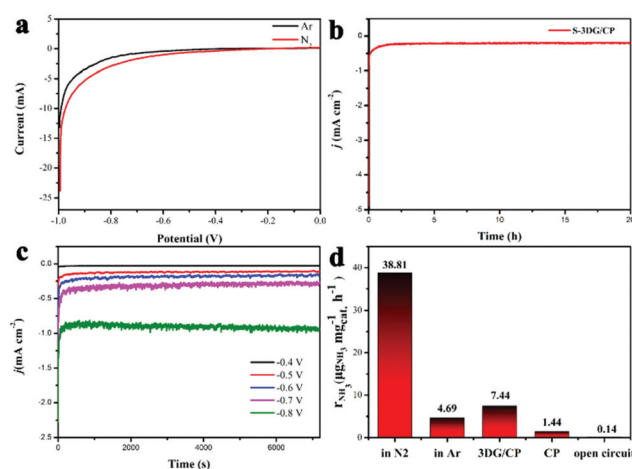


Fig. 5 (a) LSV curves of S-3DG/CP in Ar and N₂ saturated 0.05 M H₂SO₄, respectively. (b) Long-term durability measurement of S-3DG/CP at -0.6 V for 20 h. (c) Chronoamperometric curves of S-3DG/CP at different selected potentials for 2 h. (d) NH₃ yields of after 2 h electrolysis under different conditions: -0.6 V in N₂, -0.6 V in Ar, 3DG/CP and open circuit in N₂.

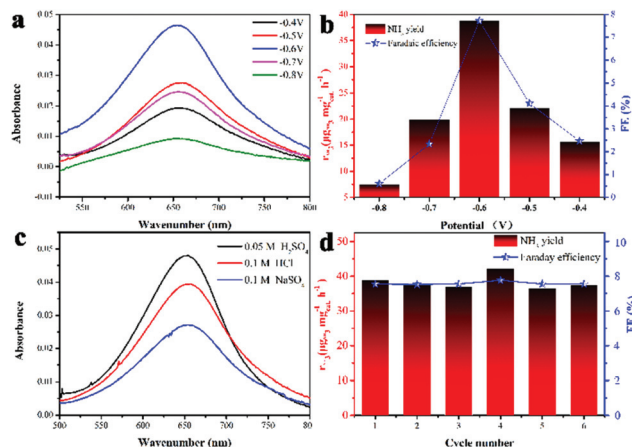


Fig. 6 (a) UV/vis absorption spectra of the electrolytes after electrolysis stained with indophenol indicator for 2 h. (b) Average NH_3 yield and faradaic efficiency for S-3DG/CP at the corresponding potential. (c) UV/vis absorption spectra of the different standard electrolytes after electrolysis stained with indophenol indicator for 2 h. (d) Faradaic efficiency and NH_3 yield during the recycling test.

electrolyte in the reaction process, we tried to use three new membranes for the electrochemical reaction under the same test conditions and satisfactory results were obtained, as shown in Fig. S11,[†] the experimental results of the new membranes is almost the same as the old.⁴⁸ It also proves that the repeatability is good. After multiple detection tests, it was proved that there was no N_2H_4 in the electrolyte after reaction.

Fig. 6a shows the UV/Vis absorption spectra of the electrolytes after electrolysis in the potential range from -0.8 to -0.4 V with indophenol indicator for 2 h. The yield of NH_3 and the corresponding FEs of the catalyst at various potentials are shown in Fig. 6b. The highest yield and FE are obtained at -0.6 V, where the value of yield is $38.81 \mu\text{g}_{\text{NH}_3} \text{mg}_{\text{cat}}^{-1} \text{h}^{-1}$ and the FE is 7.72%, which are higher than that in previous reports on non-metal catalysts for NRR. To demonstrate the high selectivity of the catalyst, after the electrochemical reaction, the NH_3 product and the possible by-product N_2H_4 in the electrolyte were spectrophotometrically determined by the indophenol blue method and the method of Watt and Chrisp, respectively. The obtained calibration curves are displayed in Fig. S13 and S14,[†] respectively. Fortunately, no hydrazine by-products were detected other than ammonia.

4. Conclusions

In summary, outstanding electrocatalytic performance of S-doped three-dimensional graphene for NRR has been proved in this work. In $0.05 \text{ M H}_2\text{SO}_4$, S-3DG/CP not merely obtains the ideal yield of $38.81 \mu\text{g}_{\text{NH}_3} \text{mg}_{\text{cat}}^{-1} \text{h}^{-1}$ and a high FE of 7.72% but also demonstrated excellent electrochemical and structural stability in the long duration N_2 -fixation reaction, which is crucial for the catalyst. This work provides more than just a highly efficient NRR catalyst and gives a method for pre-

paring the catalyst in large quantities at low temperature. Three-dimensional graphene as a substrate supported non-metal catalyst has successfully improved the conductivity of the non-metal and enhanced the stability of non-metal electrochemistry. This strongly proves the application prospect of carbon-based materials in catalyst substrates. Therefore, we are still further studying other applications of three-dimensional graphene as a substrate material in nitrogen reduction.

Conflicts of interest

There are no conflicts to declare.

Acknowledgements

The authors acknowledge the financial support of National Natural Science Foundation of China (Grant No. 21671147) and Shanxi Province Natural Science Foundation for Youths (201901D211117).

References

- 1 J. M. McEnaney, A. R. Singh, J. A. Schwalbe, J. Kibsgaard, J. C. Lin, M. Cargnello, T. F. Jaramillo and J. K. Nørskov, *Energy Environ. Sci.*, 2017, **10**, 1621.
- 2 B. H. R. Suryanto, H.-L. Du, D. Wang, J. Chen, A. N. Simonov and D. R. MacFarlane, *Nat. Catal.*, 2019, **2**, 290.
- 3 H. Kwee Lee, Y. H. Lee, C. Liu, In Y. Phang, X. Han, C.-K. Tsung and X. Yi Ling, *Sci. Adv.*, 2018, **4**, eaar3208.
- 4 X. Yan, D. Liu, H. Cao, F. Hou, J. Liang and S. X. Dou, *Small Methods*, 2019, 1800501.
- 5 F. Zhou, L. M. Azofra, M. Ali, M. Kar, A. N. Simonov, C. McDonnell-Worth, C. Sun, X. Zhang and D. R. MacFarlane, *Energy Environ. Sci.*, 2017, **10**, 2516.
- 6 B. H. R. Suryanto, C. S. M. Kang, D. Wang, C. Xiao, F. Zhou, L. M. Azofra, L. Cavallo, X. Zhang and D. R. MacFarlane, *ACS Energy Lett.*, 2018, **3**, 1219.
- 7 H.-M. Liu, S.-H. Han, Y. Zhao, Y.-Y. Zhu, X.-L. Tian, J.-H. Zeng, J.-X. Jiang, B. Y. Xia and Y. Chen, *J. Mater. Chem. A*, 2018, **6**, 3211.
- 8 C. Guo, J. Ran, A. Vasileff and S.-Z. Qiao, *Energy Environ. Sci.*, 2018, **11**, 45.
- 9 V. Kyriakou, I. Garagounis, E. Vasileiou, A. Vourros and M. Stoukides, *Catal. Today*, 2017, **286**, 2.
- 10 Y. Song, R. Peng, D. K. Hensley, P. V. Bonnesen, L. Liang, J. Huang, F. Yang, F. Zhang, R. Qiao, A. P. Baddorf, T. J. Tschaplinski, N. L. Engle, M. C. Hatzell, Z. Wu, D. A. Cullen, H. M. Meyer III, B. G. Sumpter and A. J. Rondinone, *Sci. Adv.*, 2018, **4**, e1700336.
- 11 Y. Tang, Y. Kobayashi, N. Masuda, Y. Uchida, H. Okamoto, T. Kageyama, S. Hosokawa, F. Loyer, K. Mitsuhashi, K. Yamanaka, Y. Tamenori, C. Tassel, T. Yamamoto,

- T. Tanaka and H. Kageyama, *Adv. Energy Mater.*, 2018, **8**, 1801772.
- 12 J. Wu, J. Li, Y. Gong, M. Kitano, T. Inoshita and H. Hosono, *Angew. Chem., Int. Ed.*, 2019, **58**, 825.
- 13 Z. Wang, Y. Li, H. Yu, Y. Xu, H. Xue, X. Li, H. Wang and L. Wang, *ChemSusChem*, 2018, **11**, 3480.
- 14 D. Bao, Q. Zhang, F. L. Meng, H. X. Zhong, M. M. Shi, Y. Zhang, J. M. Yan, Q. Jiang and X. B. Zhang, *Adv. Mater.*, 2017, **29**.
- 15 Y. Yao, S. Hu, W. Chen, Z.-Q. Huang, W. Wei, T. Yao, R. Liu, K. Zang, X. Wang, G. Wu, W. Yuan, T. Yuan, B. Zhu, W. Liu, Z. Li, D. He, Z. Xue, Y. Wang, X. Zheng, J. Dong, C.-R. Chang, Y. Chen, X. Hong, J. Luo, S. Wei, W.-X. Li, P. Strasser, Y. Wu and Y. Li, *Nat. Catal.*, 2019, **2**, 304.
- 16 M. Nazemi, S. R. Panikkanvalappil and M. A. El-Sayed, *Nano Energy*, 2018, **49**, 316.
- 17 H. Tao, C. Choi, L.-X. Ding, Z. Jiang, Z. Han, M. Jia, Q. Fan, Y. Gao, H. Wang, A. W. Robertson, S. Hong, Y. Jung, S. Liu and Z. Sun, *Chem*, 2019, **5**, 204.
- 18 S. Back and Y. Jung, *Phys. Chem. Chem. Phys.*, 2016, **18**, 9161.
- 19 Y. Tian, D. Xu, K. Chu, Z. Wei and W. Liu, *J. Mater. Sci.*, 2019, **54**, 9088.
- 20 P. Chen, N. Zhang, S. Wang, T. Zhou, Y. Tong, C. Ao, W. Yan, L. Zhang, W. Chu, C. Wu and Y. Xie, *Proc. Natl. Acad. Sci. U. S. A.*, 2019, **116**, 6635.
- 21 Y. Ogura, K. Sato, S. I. Miyahara, Y. Kawano, T. Toriyama, T. Yamamoto, S. Matsumura, S. Hosokawa and K. Nagaoka, *Chem. Sci.*, 2018, **9**, 2230.
- 22 Z. Wang, F. Gong, L. Zhang, R. Wang, L. Ji, Q. Liu, Y. Luo, H. Guo, Y. Li, P. Gao, X. Shi, B. Li, B. Tang and X. Sun, *Adv. Sci.*, 2019, **6**, 1801182.
- 23 L. Zhang, X. Ji, X. Ren, Y. Ma, X. Shi, Z. Tian, A. M. Asiri, L. Chen, B. Tang and X. Sun, *Adv. Mater.*, 2018, **30**, e1800191.
- 24 Y. Zhang, W. Qiu, Y. Ma, Y. Luo, Z. Tian, G. Cui, F. Xie, L. Chen, T. Li and X. Sun, *ACS Catal.*, 2018, **8**, 8540.
- 25 W. Qiu, X. Y. Xie, J. Qiu, W. H. Fang, R. Liang, X. Ren, X. Ji, G. Cui, A. M. Asiri, G. Cui, B. Tang and X. Sun, *Nat. Commun.*, 2018, **9**, 3485.
- 26 X. Zhang, T. Wu, H. Wang, R. Zhao, H. Chen, T. Wang, P. Wei, Y. Luo, Y. Zhang and X. Sun, *ACS Catal.*, 2019, **9**, 4609.
- 27 Y. Wang, K. Jia, Q. Pan, Y. Xu, Q. Liu, G. Cui, X. Guo and X. Sun, *ACS Sustainable Chem. Eng.*, 2018, **7**, 117.
- 28 C. Chen, D. Yan, Y. Wang, Y. Zhou, Y. Zou, Y. Li and S. Wang, *Small*, 2019, **15**, e1805029.
- 29 S. Chen, S. Perathoner, C. Ampelli, C. Mebrahtu, D. Su and G. Centi, *Angew. Chem., Int. Ed.*, 2017, **56**, 2699.
- 30 L. Xia, X. Wu, Y. Wang, Z. Niu, Q. Liu, T. Li, X. Shi, A. M. Asiri and X. Sun, *Small Methods*, 2018, **3**, 1800251.
- 31 H. Chen, X. Zhu, H. Huang, H. Wang, T. Wang, R. Zhao, H. Zheng, A. M. Asiri, Y. Luo and X. Sun, *Chem. Commun.*, 2019, **55**, 3152.
- 32 L. Xia, J. Yang, H. Wang, R. Zhao, H. Chen, W. Fang, A. M. Asiri, F. Xie, G. Cui and X. Sun, *Chem. Commun.*, 2019, **55**, 3371.
- 33 Q. Qin, T. Heil, M. Antonietti and M. Oschatz, *Small Methods*, 2018, **2**, 1800202.
- 34 Y. Wang, X. Cui, J. Zhao, G. Jia, L. Gu, Q. Zhang, L. Meng, Z. Shi, L. Zheng, C. Wang, Z. Zhang and W. Zheng, *ACS Catal.*, 2018, **9**, 336.
- 35 Y. Cao, Y. Gao, H. Zhou, X. Chen, H. Hu, S. Deng, X. Zhong, G. Zhuang and J. Wang, *Adv. Theory Simul.*, 2018, **1**, 1800018.
- 36 B. Cui, J. Zhang, S. Liu, X. Liu, W. Xiang, L. Liu, H. Xin, M. J. Lefler and S. Licht, *Green Chem.*, 2017, **19**, 298.
- 37 Y. N. Chen, X. Zhang and Z. Zhou, *Small Methods*, 2019, 1900050.
- 38 J. Liang, Y. Jiao, M. Jaroniec and S. Z. Qiao, *Angew. Chem., Int. Ed.*, 2012, **51**, 11496.
- 39 F. Wang, Y. P. Liu, H. Zhang and K. Chu, *ChemCatChem*, 2019, **11**, 1441.
- 40 K. Chu, Y.-P. Liu, J. Wang and H. Zhang, *ACS Appl. Energy Mater.*, 2019, **2**, 2288.
- 41 X. Cui, C. Tang and Q. Zhang, *Adv. Energy Mater.*, 2018, **8**, 1800369.
- 42 J. Zhao, J. Zhou, M. Yuan and Z. You, *Catal. Lett.*, 2017, **147**, 1363.
- 43 H. Li, X. Yang, X. Wang, M. Liu, F. Ye, J. Wang, Y. Qiu, W. Li and Y. Zhang, *Nano Energy*, 2015, **12**, 468.
- 44 Q. Wu, Y. Xu, Z. Yao, A. Lin and G. Shi, *ACS Nano*, 2010, **4**, 1963.
- 45 Q. Chen, L. Zhang and G. Chen, *Anal. Chem.*, 2012, **84**, 171.
- 46 C. Li and G. Shi, *Nanoscale*, 2012, **4**, 5549.
- 47 S. Ojala, S. Pitkäaho, T. Laitinen, N. Niskala Koivikko, R. Brahmi, J. Gaálová, L. Matejova, A. Kucherov, S. Päivärinta, C. Hirschmann, T. Nevanperä, M. Riihimäki, M. Pirilä and R. L. Keiski, *Top. Catal.*, 2011, **54**, 1224.
- 48 Y. Ren, C. Yu, X. Tan, X. Han, H. Huang, H. Huang and J. Qiu, *Small Methods*, 2019, 1900474.